Dalton Transactions

A 2,2'-Bipyridine-Containing Covalent Organic Framework Bearing Rhenium (I) Tricarbonyl Moieties for CO2 reduction

Journal:	*Dalton Transactions*
Manuscript ID	DT-ART-01-2018-000125.R1
Article Type:	Paper
Date Submitted by the Author:	08-Oct-2018
Complete List of Authors:	Popov, Damir; University of Southern California, Chemistry Luna, John; University of Southern California, Chemistry Orchanian, Nicholas; University of Southern California, Chemistry Haiges, Ralf; University of Southern California, Chemistry Downes, Courtney; University of Southern California, Chemistry Marinescu, Smaranda ; University of Southern California, Chemistry

Dalton Transactions

PAPER

A 2,2'-Bipyridine-Containing Covalent Organic Framework Bearing Rhenium (I) Tricarbonyl Moieties for CO_2 Reduction†

Damir A. Popov, John M. Luna, Nicholas M. Orchanian, Ralf Haiges, Courtney A. Downes and Smaranda C. Marinescu*

The reduction of CO_2 into higher energy products such as carbon-based fuels and feedstocks is an attractive strategy for mitigating the continuous rise in CO_2 emissions associated with the growing global energy demand. Rhenium tricarbonyl complexes bearing 2,2'-bipyridine (2,2'-bpy) ligands are well-established molecular electrocatalysts for the selective reduction of CO_2 to CO. Construction of efficient devices for this electrochemical process requires the immobilization of electrocatalysts to electrode surfaces. To integrate Re(2,2'-bpy)$(CO)_3$ fragments into a covalent organic framework (COF), Re(5,5'-diamine-2,2'-bpy)$(CO)_3$Cl (**1**) was synthesized and electrochemically investigated. Complex **1** is an active and selective electrocatalyst for the reduction of CO_2 to CO with excellent faradaic efficiency (99%). The presence of the amine substituents leads to a destabilization of the π^* orbital of the 5,5'-diamine-2,2'-bpy ligand with respect to the metal center. Therefore, **1** requires more negative potentials (–2.47 V vs. $Fc^{+/0}$) to reach the doubly reduced catalytically active species. DFT studies were conducted to understand the electronic structure of **1**, and support the destabilizing effect of the amine substituents. The Re-2,2'-bpy fragments were successfully integrated into a COF containing 2,2'-bpy moieties (COF-2,2'-bpy) via a post-metallation synthetic route to generate COF-2,2'-bpy-Re. A composite of COF-2,2'-bpy-Re, carbon black, and polyvinylidene fluoride (PVDF) was readily immobilized onto glassy carbon electrodes and electrocatalytic CO_2 reduction to CO was observed at –2.8 V vs. $Fc^{0/+}$, with a faradaic efficiency of 81% for CO production.

Received 00th January 20xx,
Accepted 00th January 20xx

DOI: 10.1039/x0xx00000x

www.rsc.org/dalton

Introduction

Carbon dioxide (CO_2), a greenhouse gas that is released by both natural and artificial processes, has received attention as an abundant, economical, and renewable C_1 feedstock that can be converted to higher-energy products.[1-5] Production of renewable chemical fuels from CO_2 reduction can provide a method to store the electricity generated from solar and wind power in the form of chemical bonds, which can counteract the intrinsic intermittency of the renewable energy sources.[6] In addition, the conversion of CO_2 to chemical fuels would positively impact the global CO_2 balance.[2]

One promising route to the production of renewable chemical fuels is the electrocatalytic reduction of CO_2 (ERC). A variety of molecular catalysts have been studied for this process.[2-5, 7-9] Molecular catalysts and their intermediates are attractive because control over the first, second, and outer coordination spheres of the ligand environment allows for tuning of their chemical properties, such as reduction potentials, catalytic activity, and selectivity. Of particular promise are the rhenium 2,2'-bpy complexes. The ligands 2,2'-bpy are commonly used in coordination chemistry and form stable well-defined complexes.[10, 11] Such systems can undergo multiple reduction events with redox equivalents stored on both the metal centre and the ligand due to the redox non-innocence of 2,2'-bpy.[12, 13] Due to their high selectivity for CO_2 reduction over proton reduction, rhenium 2,2'-bpy catalysts have been extensively studied.[14-16]

Deployment of large-scale electrocatalytic devices requires the development of synthetic strategies for the immobilization of molecular catalysts to electrode surfaces. Heterogenization of molecular catalysts has emerged as a promising strategy that combines the favourable properties of molecular homogeneous systems, such as high selectivity and tunability, with the stability and robustness associated with heterogeneous catalysts. Demonstrated methods for the immobilization of molecular CO_2 reduction electrocatalysts onto carbon-based electrodes include casting methods[15, 17-20], the use of pyrene groups[21-23], covalent attachment[24-26], electropolymerization[15, 27-31], and incorporation of catalytic units into extended frameworks[32-35]. Immobilization of molecular electrocatalysts via metal-organic frameworks (MOFs) and covalent-organic frameworks (COFs) is an

Department of Chemistry, University of Southern California, Los Angeles, CA, 90089, USA. E-mail: smarines@usc.edu

† Electronic Supplementary Information (ESI) available: Additional crystallographic data, molecular orbital images, spectroscopic characterization, and electrochemical data. See DOI: 10.1039/x0xx00000x

attractive strategy because the permanent porosity of these materials allows for rapid substrate diffusion and access to an unprecedented number of active sites leading to enhanced catalytic activity in comparison with solution-based molecular electrocatalysts.[33-46] Additionally, site-isolation of the molecular catalysts incorporated in MOFs and COFs results in enhanced stability of these systems and allows for extended catalytic performance.

Strategies have been developed for the incorporation of Re(2,2'-bpy) catalytic units into heterogeneous structures for immobilization onto carbon-based supports. The non-covalent attachment of Re(2,2'-bpy) complexes containing pyrene groups onto highly oriented pyrolytic graphite (HOPG) electrodes was presented by Gray et al.[21] The resulting device was shown to be active towards the electrochemical reduction of CO_2 to CO, however, long-term performance was limited by leaching of the rhenium active sites into solution. Similarly, an analogous Mn(2,2'-bpy) complex was anchored via a pyrene unit to a carbon nanotube electrode yielding an assembly that displays high activity for ERC under fully aqueous conditions with TONs of up to 1790 ± 290 for CO and up to 3920 ± 230 for formate.[23] Covalent attachment is exemplified by graphite-conjugated Re(2,2'-bpy) (GCC-Re) catalysts, where the authors used the *o*-quinone moieties, commonly found on the edge planes of graphite, to condense *o*-phenyldiamine units of a modified Re(2,2'-bpy) complex.[26] The resulting GCC-Re surfaces exhibit high turnover numbers (>12,000) and turnover frequencies, exceeding the activity of the soluble molecular analogue. Controlled current electrolysis of GCC-Re revealed sustained catalytic activity at 1 mA/cm^2 for 1.4(3) h, followed by rapid deactivation. To our knowledge, the only example of Re(2,2'-bpy) incorporation into a MOF for ERC was developed by Sun and co-workers. The monolithic Re-based MOF thin film was deposited onto conductive FTO substrates by liquid-phase epitaxy.[47] The device demonstrated high current densities that exceeded 2 mA/cm^2,[33, 35] however the current densities in a CO_2-saturated solution gradually dropped off, which was attributed to degradation of the MOF. Additionally, metal 2,2'-bpy catalysts have been incorporated into MOFs for photocatalytic H_2 evolution, photocatalytic carbon dioxide reduction, and electrocatalytic water oxidation.[46, 48-53] However, ERC was not reported in these studies.

We sought to investigate crystalline porous frameworks, in particular covalent organic frameworks (COFs), as tunable materials for electrocatalysis.[54] These materials are advantageous because they can be easily constructed from molecular building blocks, thus enabling the control of the arrangement of catalytic active sites within the COF structure. Moreover, the pores surrounding the active sites would provide access for the substrate, in this case CO_2, to the catalytic site. Here, we show the incorporation of catalytic rhenium 2,2'-bpy active sites into a COF. In this study, we use a previously reported COF (COF-2,2'-bpy) derived via the modified Schiff base reaction between 1,3,5-triformylphloroglucinol and 2,2'-bipyridine-5,5'-diamine, which combines reversible and irreversible Schiff base reactions.[54, 55] An irreversible proton tautomerism leads to the formation of COF-2,2'-bpy, with remarkable stability in water, as well as strong acids and bases. Therefore, the resulting framework can serve as a platform for catalysis under harsh conditions, which was demonstrated in the study of COF-2,2'-bpy-supported Co catalyst for the electrocatalytic oxygen evolution reaction (OER).[56] This catalyst demonstrated high stability (24 h) and efficiency (95%).

With this in mind, a Re(2,2'-bpy) complex is proposed, where the 2,2'-bpy fragment is modified with amine groups in the 5,5' positions for subsequent integration into a COF. The synthesis, characterization and electrocatalytic properties of Re(2,2'-bpy-5,5'-diamine)$(CO)_3Cl$ (**1**) towards CO_2 reduction is presented. The electronic effects of the amine groups are probed using DFT. Two different synthetic pathways, a direct Schiff base condensation with **1**, and post-metallation of COF-2,2'-bpy are explored for the integration of **1** into a COF structure. The resulting materials are studied as electrocatalysts for CO_2 reduction.

Results and discussion

Synthesis and Characterization

Treatment of $Re(CO)_5Cl$ with 2,2'-bipyridine-5,5'-diamine led to the formation of a yellow precipitate. The ^{1}H NMR spectrum of the 2,2'-bpy-5,5'-diamine ligand displays peaks at δ 7.89, 7.84 and 6.95 ppm, corresponding to the aromatic protons, and a broad singlet peak at δ 5.30 ppm, corresponding to the amine protons. Upon metallation, a downfield shift in the peaks is observed (δ 8.22, 7.96, 7.21, and 6.20 ppm), suggesting clean formation of complex **1** with a deshielding effect of the rhenium tricarbonyl moieties (Equation 1). Solid state structure of **1**•DMF reveals equatorial coordination of the bipyridine ligand with a N(1)–Re(1)–N(2) angle of 75.40(5)°, and *facial* arrangement of the three carbonyl ligands, typical of other Re(I)-tricarbonyl complexes bearing 2,2'-bpy ligands (Figure 1 and Tables S1–S3). The similarity in geometry between **1** and Re(2,2'-bpy)$(CO)_3Cl$ suggests that incorporation of the *meta*-substituents does not influence the geometry of the Re center, as has been confirmed by X-ray crystallography.

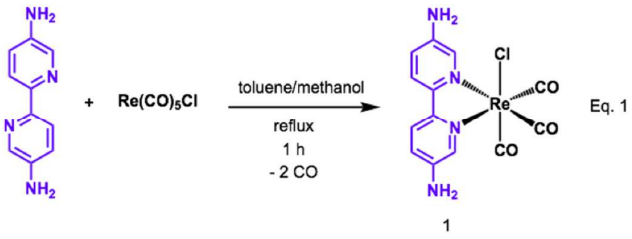

Eq. 1

1

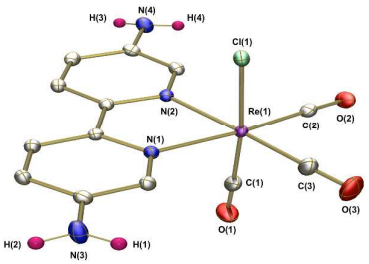

Figure 1. Solid state structure of **1**•DMF with ellipsoids set at 50% probability level. Aryl protons and the solvent molecule (DMF) are omitted for clarity.

FTIR studies of a pellet of **1** with KBr reveal two major frequencies at 2015 and 1896 cm^{-1}, which are characteristic of CO stretching frequencies (Figure S1). The frequency at 2015 cm^{-1} is assigned to the stretching mode of the axial CO ligand; while the broad frequency at 1896 cm^{-1} is indicative of two overlapping equatorial CO stretches. Besides these features, the FTIR spectrum displays additional shoulders at 2022, 1929, and 1845 cm^{-1}. However, when the FTIR spectrum of complex **1** was collected using an ATR attachment (Figure 2), two major peaks at 2011 cm^{-1} and 1891 cm^{-1} were observed, suggesting that **1** undergoes halogen exchange with KBr during the pellet preparation. The minor peaks at 1919 and 1836 cm^{-1} correspond to the in-phase and out-of-phase stretching modes of the equatorial CO ligands, and these frequencies persist in the ATR-IR spectrum. The broad peak at 1891 cm^{-1} is a fundamental band and the appearance of the persisting shoulders is due the coupling caused by Fermi resonance. A classic example is benzoyl chloride.[57] Additionally, similar shoulders have been observed for $Re(bpy\text{-}COOH)(CO)_3Cl$ by Kubiak et al.[16]

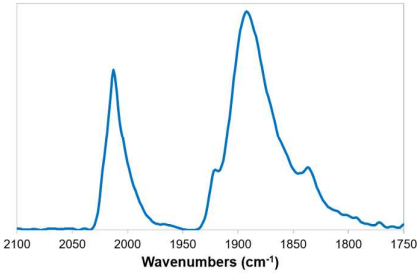

Figure 2. CO stretching region of the ATR-FTIR spectrum of **1**.

To provide computational insight for the assignments of the carbonyl stretching modes, frequency calculations were run at the M06 level of theory with a hybrid basis set (6-31G* for C, H, N, O and LANL2DZ for Cl, Re). The calculated carbonyl stretching frequencies for $Re(2,2'\text{-}bpy)(CO)_3Cl$ and **1** are shown in Table S4, and the stretching vectors for these modes are depicted in Figure S2. The character of these three modes and their relative energy ordering are unchanged in **1**, providing theoretical support for the assignment of the experimental FT-IR results.

An increase in the donor strength of the 2,2'-bpy-5,5'-diamine ligand is expected to decrease the Re-N bond lengths due to the stronger nitrogen donors, while the carbonyl C-O bond length should increase due to stronger π-backbonding interactions with Re. As neither the Re-N, nor the C-O bond lengths are perturbed, it can be inferred that the electron density at Re is largely unchanged by the inclusion of electron-donating amine groups in the *meta*-positions (Table S4). However, there is a consistent decrease in the experimental and calculated carbonyl stretching frequencies upon inclusion of the *meta*-substituted amines, suggesting that there is a subtle increase in π-backbonding from rhenium to the carbonyl ligands, which was less evident from the structural parameters.

High resolution (HR) XPS studies of **1** reveal the presence of Re, Cl, and N (Figure 3). One set of peaks is observed in the Re 4f region, with binding energies of 43.4 and 40.9 eV, corresponding to Re $4f_{5/2}$ and $4f_{7/2}$ levels, respectively. HR XPS studies in the Cl 2p region reveal two peaks, with binding energies of 198.9 and 197.1 eV, and assigned to Cl $2p_{1/2}$ and $2p_{3/2}$ levels, respectively. Additionally, one peak at 398.8 eV was observed and assigned to the N 1s level.

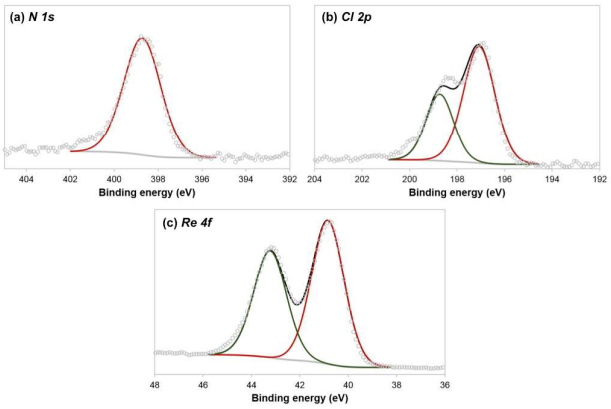

Figure 3. XPS spectra of **1**. (a) N 1s core level; (b) Cl 2p core level; and (c) Re 4f core level.

Electrochemical Studies

Cyclic voltammograms (CVs) of **1** were recorded using glassy carbon electrodes in acetonitrile (MeCN) solutions of 0.1 M $[n\text{Bu}_4\text{N}][PF_6]$ under a nitrogen atmosphere, and multiple scans of **1** display similar current density values (Figures 4 and S21). Two irreversible reduction features are observed at –2.11 V and –2.47 V vs. $Fc^{0/+}$ (Figure 4). All the potentials listed here are referenced versus $Fc^{0/+}$ couple. These reduction features do not exhibit increased reversibility upon either increasing the scan rate (Figure S3), or reversing the potential after the first reduction (Figure S22). The cathodic peak current densities at –2.11 V and –2.47 V are directly proportional to the square root of the scan rate (Figure S4), as expected for a

freely diffusing species in solution obeying the Randles-Sevcik equation.

CVs of **1** under CO_2 exhibit a ~4-fold increase in current density near the second reductive feature, suggesting that a catalytic reaction is taking place (Figure 4). Controlled potential electrolysis (CPE) of **1** (0.5 mM) under CO_2 was performed at –2.57 V (Figure S5). 9.2 coulombs of charge were consumed after 1 h. Analysis of the gas mixture confirmed production of CO with a Faradaic efficiency (FE) of 99% and a TON of 100,800, as described in the SI (Table S5). Negligible amounts of CO were observed under a nitrogen atmosphere, suggesting that the CO produced is from CO_2 and not from the carbonyl groups present in **1**. Negligible amounts of formate were observed by FTIR, suggesting that the overall reaction is a 2-proton 2-electron reduction of CO_2 to CO.[58] Addition of external proton donors (e.g. water, methanol, trifluoroethanol, and phenol) did not improve the catalytic performance. At the negative reduction potentials needed for the catalysis, it has been reported that the O-acceptor can be a proton extracted from MeCN[59] or from [nBu$_4$N][PF$_6$] through Hoffman degradation[60]. The FTIR spectra of the electrolysis solutions before and after CPE studies display identical peaks (Figure S6), suggesting that complex **1** is stable under the electrocatalytic conditions.[61-63]

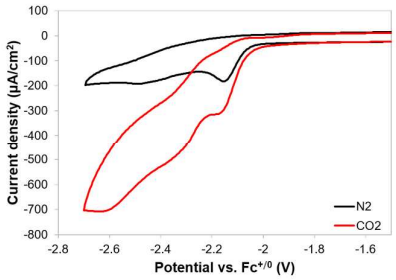

Figure 4. CVs of **1** (0.5 mM) in 0.1 M [nBu$_4$N][PF$_6$] in MeCN under Ar (black) and CO_2 (red) at a scan rate of 100 mV/s.

The reduction features in **1** occur at potentials more negative than those of any of the previously reported rhenium 2,2'-bpy molecular catalysts (Table S6).[16, 64] To understand this difference in the electronics of **1**, DFT calculations were performed. Relative energies for the Kohn-Sham molecular orbitals of Re(2,2'-bpy)(CO)$_3$Cl and **1**, along with illustrations of the respective HOMOs and LUMOs, are presented in Figure 5. It is clear from this diagram that the overall HOMO and LUMO character for **1** is not drastically perturbed from that of Re(2,2'-bpy)(CO)$_3$Cl. The LUMO retains its 2,2'-bpy π^* character, and the HOMO exhibits Re-Cl π^* character. Though the character of these orbitals is not perturbed, the LUMO is evidently destabilized by the increased antibonding interactions in the π-framework of the 5,5'-diamine-2,2'-bpy ligand. This destabilization is the likely cause for the increased reduction potential of **1** relative to Re(2,2'-bpy)(CO)$_3$Cl, as the additional electron would populate this destabilized, higher-lying LUMO. The relative energy of the corresponding 2,2'-bpy-5,5'-diamine π-bonding orbital was also shown to lie higher in energy than that of Re(2,2'-bpy)(CO)$_3$Cl (see Figure S11), confirming that the highest occupied 2,2'-bpy-5,5'-diamine based orbital is similarly destabilized upon introduction of the amine groups.

These predictions are consistent with the experimental evidence provided that the observed reduction events are 2,2'-bpy based. In order to demonstrate this, the zinc analogue of **1**, Zn(2,2'-bpy-5,5'-diamine)(CH$_3$COO)$_2$·H$_2$O, was synthesized by treating zinc acetate with 2,2'-bpy-5,5'-diamine in water/methanol to generate a white solid. The ^{1}H NMR spectrum of this solid displays peaks corresponding to the 2,2'-bpy-5,5'-diamine ligand environment, along with another peak at 1.79 ppm, corresponding to the methyl protons in the acetate group (6H). The electrochemistry of the zinc complex was explored (Figure S10). Two reduction events are observed at -2.31 V and -2.71 V, suggesting that the features present in Figure 4 might be ligand-based reductions, which is common for related 2,2'-bpy based Re complexes.

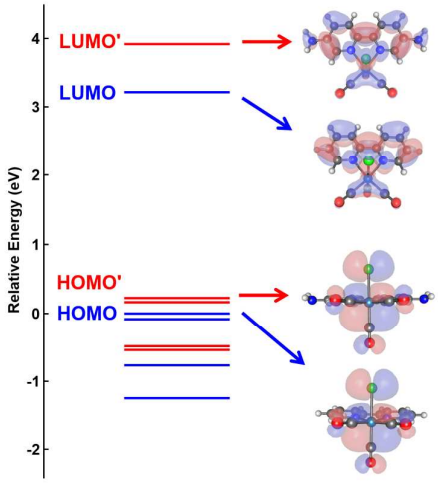

Figure 5. Molecular orbital diagrams and frontier orbital images for Re(2,2'-bpy)(CO)$_3$Cl (HOMO, LUMO; blue) and **1** (HOMO', LUMO'; red). Calculations were performed using the M06 functional with the 6-311G* basis set for H, C, N, and O atoms and the LANL2DZ effective core potential and basis set for Cl and Re atoms.

According to published mechanistic studies of CO_2 reduction with Re(2,2'-bpy)(CO)$_3$Cl, it is common for this and related 2,2'-bpy based Re complexes to dissociate Cl$^-$ following the electron transfer step.[58, 65-73] The species formed upon the electron transfer, [Re(2,2'-bpy)(CO)$_3$Cl]$^-$, exists in equilibrium with the neutral complex, [Re(2,2'-bpy)(CO)$_3$]^0, and the dissociated Cl$^-$. Since the first reduction feature in **1** appears irreversible at various scan rates (Figure S3), this indicates that chloride dissociation is an irreversible process on the timescale of the CV experiment. The complete chloride dissociation in **1** is attributed to the more cathodic potential of the first reduction caused by the destabilization of the LUMO (*vide supra*).

To probe this observed irreversibility, changes in the CV response upon addition of nBu$_4$NCl were monitored. The addition of nBu$_4$NCl is expected to shift the equilibrium away from the dissociation of chloride, causing an increase in the reversibility of the first reduction feature. This, however, is not observed even in the presence of a large excess of chloride (0.1 M nBu$_4$NCl), supporting that the observed chloride dissociation is indeed an irreversible process (Figure S7). To further probe the irreversibility of the first reduction feature in **1**, a chloride-abstracted analogue of **1**, Re(2,2'-bpy-5,5'-diamine)(CO)$_3$(MeCN)(OTf) (**1**^{OTf}), was synthesized from **1** and silver triflate. The ^{1}H NMR spectrum of the resulting crystals display peaks associated with the 2,2'-bpy-5,5'-diamine ligand environment along with a broad peak at 2.09 ppm (3H), indicative of the coordinated acetonitrile ligand. The reduction features observed in **1**^{OTf} are more positive compared to the ones in **1**, by approximately 200 mV and 190 mV, respectively (Figure S8), consistent with other previously reported triflate rhenium bipyridine complexes.[64, 74] No increase in reversibility of the first reduction feature in **1**^{OTf} is observed upon increasing scan rate (Figure S9), suggesting irreversible loss of the acetonitrile ligand following the first reduction on the CV timescale. Therefore, both experiments using nBu$_4$NCl and **1**^{OTf} support that the first reduction and the subsequent ligand (Cl^- or MeCN) loss is an irreversible process.

Immobilization studies

Following the successful electrocatalytic reduction of CO_2 to CO using **1**, attempts to integrate **1** into a COF by a modified Schiff base condensation were explored.[55, 56, 75] In this reaction the initial imine formation is followed by an irreversible enol-to-keto tautomerism, which leads to a two-dimensional COF with remarkable stability in water, strong acids, and bases. Inspired by this and the fact that the 2,2'-bpy-5,5'-diamine ligand was successfully used as a building block for COF (COF-2,2'-bpy) formation,[56, 75] we reasoned that the structurally related complex **1** could induce COF formation in a similar fashion. Unfortunately, attempts to directly utilize **1** were unsuccessful and led to unidentifiable mixtures.

Since COF-2,2'-bpy contains 2,2'-bpy fragments, it was proposed that post-synthetic modification[76-78] of this framework, specifically post-metallation, could result in incorporation of the rhenium (I) tricarbonyl fragments (Re(CO)$_3$), effectively heterogenizing the rhenium 2,2'-bpy molecular catalyst. We prepared COF-2,2'-bpy, which is an orange crystalline material featuring an intense peak at 2 θ = 3.6° in the powder X-ray diffraction (PXRD) pattern, corresponding to the [100] reflection.[56, 75] Treatment of COF-2,2'-bpy with Re(CO)$_5$Cl in toluene under reflux for 3 days results in the formation of a dark-red powder, COF-2,2'-bpy-Re, which underwent solvent exchange to remove the excess starting materials (Equation 2). The amount of Re catalyst incorporated into the framework can be modified by varying the Re(CO)$_5$Cl/COF-2,2'-bpy ratio. Using ratios of 0.01, 0.05, 0.15, 1.0, and 1.5 results in the formation of COF-2,2'-bpy-Re samples with rhenium weight percentages of 0.21, 0.65, 1.86, 15.39 and 29.38, respectively, as determined by inductively coupled plasma atomic emission spectroscopy (ICP-OES) studies of the digested dark-red powders. FTIR and XPS studies were used to probe whether molecular, well-defined, Re centres exist within COF-2,2'-bpy-Re.

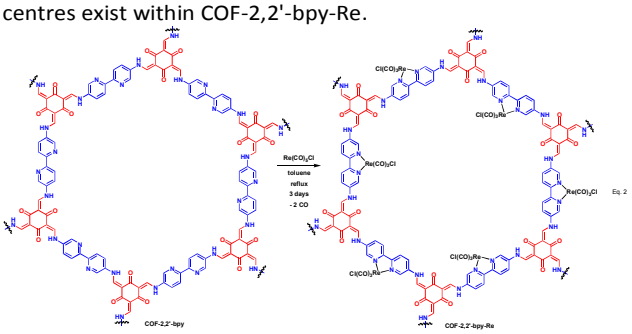

The FTIR spectra of all the COF-2,2'-bpy-Re samples displayed the presence of the characteristic CO stretches at 2023 and 1907 cm^{-1} (Figure 6). The former is assigned to the stretching mode of the axial CO ligand, and the latter is assigned to the in-phase and out-of-phase stretching modes of the equatorial CO stretches (unresolved due to their similar energies), which agrees with the FTIR of **1** (*vide supra*), suggesting that Re(CO)$_3$ sites retain their molecular nature within the heterogeneous framework. No CO stretches were observed in the FTIR spectrum of COF-2,2'-bpy (Figure S12). Additionally, the CO stretches in the FTIR spectrum of Re(CO)$_5$Cl (Figure S13) are distinct from those of COF-2,2'-bpy-Re, indicating that 2,2'-bpy-coordinated Re(CO)$_3$ moieties are the source of the CO stretches observed in Figure 6.

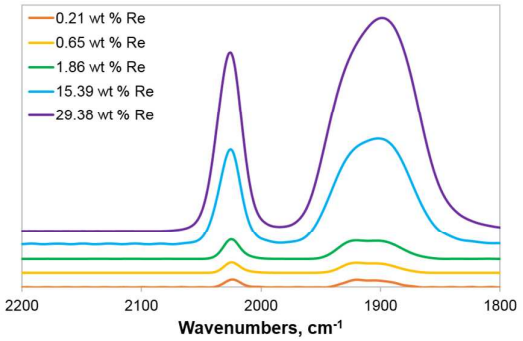

Figure 6. Overlay of the FTIR spectra of COF-2,2'-bpy-Re with various amounts of incorporated rhenium, such as: 0.21 (orange), 0.65 (yellow), 1.86 (green) 15.39 (blue), and 29.38 (purple) wt % Re.

HR XPS studies of COF-2,2'-bpy-Re 15.39 and 29.38 wt % Re reveals the presence of Re, Cl, and N (Figures S14 and 7). One set of peaks is observed in the Re 4f region with binding energies of 44.3 and 41.9 eV, corresponding to Re 4f$_{5/2}$ and 4f$_{7/2}$ levels. The XPS peaks observed are similar to the ones of **1**, as well as to those of other reported heterogenized species,[21, 26] suggesting that the rhenium tricarbonyl moiety is maintained upon heterogenization via COF. HR XPS studies of

the Cl 2p region reveal two peaks, with binding energies at 198.9 and 198.2 eV, corresponding to Cl $2p_{1/2}$ and $2p_{3/2}$, respectively. Additionally, one peak at 400.5 eV was observed and assigned to the N 1s region. XPS studies of $Re(CO)_5Cl$ (Figure S15) show distinct electronic environments for both the Re 4f and Cl 2p regions from that of COF-2,2'-bpy-Re. Therefore, based on the FTIR and XPS data for COF-2,2'-bpy-Re, we conclude that Re-2,2'-bpy are incorporated into the framework.

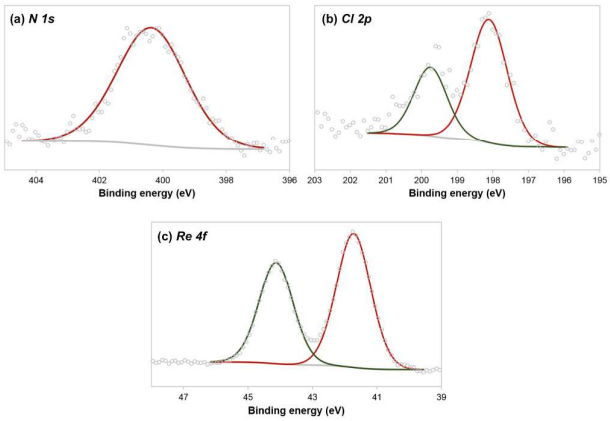

Figure 7. XPS spectra of COF-2,2'-bpy-Re that displays 29.38 wt % Re. (a) N 1s core level; (b) Cl 2p core level; (c) Re 4f core level.

To probe whether the structural integrity of COF-2,2'-bpy was retained upon post-metallation, PXRD patterns were collected for all the COF-2,2'-bpy-Re samples and the un-metallated COF-2,2'-bpy (Figure 8). All the COF-2,2'-bpy-Re samples except for the 29.38 wt % Re sample maintained the crystalline structure of COF-2,2'-bpy as evidenced by retention of the peak at 2 θ = 3.6°. The loss of this peak in the 29.38 wt % Re case is consistent with the lack of long-range order due to a high occupancy of the 2,2'-bpy active sites by Re tricarbonyl fragments, which induces exfoliation and pore misalignment.

The permanent porosity of COFs is an attractive feature that is expected to facilitate substrate diffusion. To investigate the surface areas of the developed frameworks, Brunauer-Emmett-Teller (BET) measurements were performed. The surface areas of COF-2,2'-bpy-Re 15.39 and 29.38 % were found to be 192.7 and 150.0 m^2/g, respectively, which is smaller that the surface area found for COF-2,2'-bpy-supported Co material (450 m^2/g).[56] The small pore size of the resulting COF-2,2'-bpy-Re samples could lead to poor diffusion of CO_2 throughout the material, thus inhibiting electrocatalysis.

Having observed successful incorporation of $Re(CO)_3$ fragments into COF-2,2'-bpy, the efficiency of the resulting materials as catalysts for ECR was explored. Given that many framework materials are insulating,[47, 79, 80] and that an analogous Co catalyst hosted by COF-2,2'-bpy was supported on a highly conductive carbon-based material,[56] we decided to integrate COF-2,2'-bpy-Re with a conductive additive, carbon black, and a polymer binder, such as polyvinylidene fluoride (PVDF), to generate the COF-2,2'-bpy-Re-based composite. CVs of the glassy carbon electrode modified with the rhenium-based composite in MeCN (0.1 M [nBu$_4$N][PF$_6$]) under N_2 display no redox features. A similar behavior was reported by Surendranath et al. for the surface-bound Re(2,2'-bpy) species.[26]

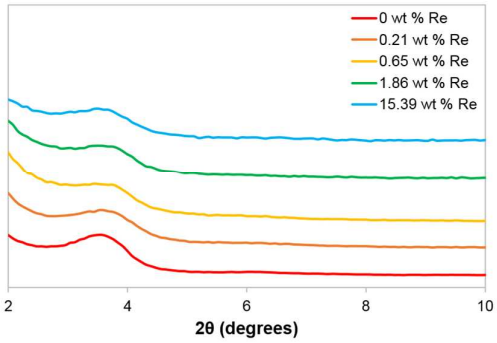

Figure 8. Overlay of the experimental PXRD patterns of COF-2,2'-bpy-Re with 0.00 (red), 0.21 (orange), 0.65 (yellow), 1.86 (green) and 15.39 (blue) wt % Re incorporation.

For the COF-2,2'-bpy-Re samples with 0.21, 0.65, 1.86, and 15.39 wt % Re, all of which possessed the crystallinity of the parent COF-2,2'-bpy, minimal current increases were observed for CV experiments under a CO_2 atmosphere and no CO was detected by GC following electrolysis. However, the CV of the composite based on COF-2,2'-bpy-Re 29.38 wt % Re, termed **2**, displays currents reaching 13.2 mA at a potential of –2.8 V under CO_2 saturation (Figure 9). In comparison, composite **2** displays a current of 4.8 mA at the same potential under N_2. The observed current enhancement for composite **2** under CO_2 suggests that a catalytic reaction is taking place.

CPE of **2** was performed in MeCN (0.1 M [nBu$_4$N][PF$_6$]) under a CO_2 atmosphere in a sealed H-cell at –2.8 V vs. $Fc^{0/+}$ (Figure S16). During 1 hour of electrolysis, aliquots of the gaseous headspace were taken at the 30 min and 60 min intervals and analyzed by GC. GC confirmed the formation of CO, with an 81% faradaic efficiency at 30 min and 57% at 60 min (Table S8). The amount of CO detected at 30 min was the same as the amount of CO at 60 min, suggesting low stability of the catalyst under prolonged electrolysis. The CPE profile exhibits a significant drop-off in current, similar to that of the reported Re-GCC.[26] Control experiments performed under CO_2 with composites based on COF-2,2'-bpy and $Re(CO)_5Cl$, or carbon balck and PVDF, led to negligible amounts of CO detected, suggesting that none of these are catalysts for ECR (Figure S17). Additionally, CPE experiments of **2** under N_2 resulted in no CO production, indicating the absence of non-catalytic sources of CO. Together, these data indicate that **2** is responsible for the ECR observed.

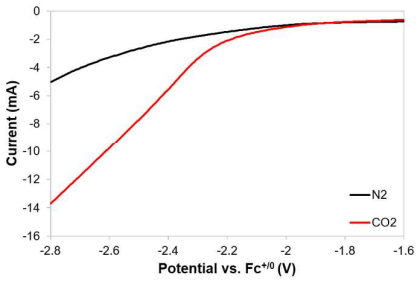

Figure 9. Polarization curves for composite **2** in a 0.1 M [nBu$_4$N][PF$_6$] acetonitrile solution under N_2 (black) and CO_2 (red) at a scan rate of 10 mV/s.

Comparison of the CVs before and after CPE confirmed the instability of **2** (Figure S18). Limited stability of other heterogenized Re(2,2'-bpy) molecular catalysts has been previously observed. [21, 26, 47] A possible deactivation pathway in **2** is leaching of rhenium into solution during the CPE studies. This was probed using ICP-OES analysis of the solution generated after CPE experiments, however, negligible amounts of rhenium were detected. Electrolyzing the postcatalysis solution with a clean glassy carbon electrode under CO_2 showed background currents (Figure S19), typical to those of the bare glassy carbon electrode in fresh electrolyte solution and did not lead to the formation of CO. Additionally, the XPS spectra of **2** following electrolysis experiments were also collected (Figure S20). The persistence of Re signals at the same binding energies as those observed for **2** prior catalysis indicates that the Re active sites are retained after catalysis. These data indicate that leaching of Re into solution is not responsible for the loss of catalytic activity. A possible decomposition pathway is the degradation of the framework or the composite as a whole, limiting its long-term catalytic activity.

Additionally, the ability of composite **2** to achieve high electrocatalytic activity is limited by its weak non-covalent interactions with the electrode surface. Additionally, the polymer binder used here, PVDF, swells in acetonitrile, disrupting the electrical integration between the catalyst, carbon black, and the electrode surface, resulting in a surface assembly with poor conductivity and charge transfer. Low surface areas of the resulting material may also prevent mass transport of the substrate (CO_2) to the rhenium active sites, and/or product diffusion, inhibiting efficient catalysis. Overall, poor charge and mass transport are suspected to be the main factors limiting the electrocatalytic activity and leading to the poor performance of the COF-2,2'-bpy-Re composites for CO_2 reduction.

Conclusions

In summary, we report here the synthesis of Re(2,2'-bpy-5,5'-diamine)(CO)$_3$Cl (**1**), and its investigation towards the electrocatalytic CO_2 reduction. Complex **1** reduces CO_2 to CO at –2.57 V with a faradaic efficiency of 99% during 1 hour of electrolysis. DFT studies were employed to investigate the electronic structure of **1** and predicted that the LUMO of **1** is destabilized relative to that of Re(2,2'-bpy)(CO)$_3$Cl. This destabilization perturbs the electrochemical behaviour of **1** as the complex displays more negative and irreversible reduction features in comparison to Re(2,2'-bpy)(CO)$_3$Cl. This, in turn, leads to irreversible chloride dissociation as the population of the destabilized higher-lying LUMO necessitates a more negative reduction potential.

Efforts to heterogenize **1** by incorporation into the COF-2,2'-bpy framework containing unmetallated 2,2'-bpy moieties led to the isolation of COF-2,2'-bpy-Re. A series of FTIR and XPS experiments showed the presence of well-defined rhenium sites in a single homogeneous environment. The ratio of Re incorporation is varied between 0.21 and 29.38 wt % Re. When COF-2,2'-bpy-Re is utilized as a composite with carbon black and PVDF, only the sample with the highest rhenium concentration, 29.38 wt % Re, was shown to be active for ERC to CO at –2.8 V. Following a 30 min CPE, CO was produced with a faradaic efficiency of 81%. The electrocatalytic activity of the composite was diminished after 30 min of electrolysis, and attributed to inhibited mass transport and substrate diffusion.

Experimental Section

General considerations

All manipulations of air and moisture sensitive materials were conducted under a nitrogen atmosphere on a dual manifold Schlenk line. The glassware was oven-dried prior to use. Acetonitrile and toluene were degassed with nitrogen and passed through activated alumina columns and stored over 4 Å Linde-type molecular sieves. Deuterated solvents were dried over 4 Å Linde-type molecular sieves prior to use. ^{1}H NMR spectra were acquired at room temperature using Varian spectrometers and referenced to the residual ^{1}H resonances of the deuterated solvent (^{1}H: $CDCl_3$, d 7.26 ppm; DMSO-d_6, δ 2.50 ppm). Elemental analyses were performed by Robertson Microlit Laboratories, Ledgewood, New Jersey. All the chemical reagents purchased from commercial vendors and were used without further purification. Commercially available tetrabutylammonium hexafluorophosphate ([nBu$_4$N][PF$_6$]) was recrystallized from hot methanol prior to use. Compounds 2,2'-bpy-5,5'-diamine[81, 82] and 2,4,5-trihydrobenzene-1,3,5-tricarbaldehyde,[83] and the porous framework COF-2,2'-bpy[55] were prepared according to the reported literature procedures. The isolation of 2,2'-bpy-5,5'-diamine from the corresponding dihydrochloride was performed with slight modifications from the reported literature procedures[82]. The isolated dihydrochloride was dissolved in the minimal amount of water and the solution was treated with concentrated ammonia. This treatment allowed for the formation of needle-like crystals of the diamine (70 %).

Physical methods

Powder X-ray diffraction (PXRD) was performed on a Rigaku Ultima IV X-ray diffractometer in reflectance parallel beam/parallel slit alignment geometry. The measurement employed Cu Ka line focused radiation at 1760 W (40 kV, 44 mA) power and a Ge crystal detector fitted with a 0.6 mm radiation entrance slit. Samples were mounted on zero-background sample holders. Samples were observed using a 1° 2 θ step scan from 2.0° to 60.0° with an exposure time of 11.4 s per step. No peaks could be resolved from the baseline for 2 θ > 35°.

Inductively coupled plasma optical emission spectroscopy (ICP-OES) measurements were performed using a Thermo Scientific iCAP 7000 ICP-OES. A 1000 ppm rhenium standard in nitric acid (Sigma Aldrich) was used to construct a calibration plot.

XPS data were collected using a Kratos AXIS Ultra instrument. The monochromatic X-ray source was the Al Ka line at 1486.6 eV, directed at 35° to the sample surface (55° off normal). Emitted photoelectrons were collected at an angle of 35° with respect to the sample surface (55° off normal) by a hemispherical analyzer. The angle between the electron collecting lens and the X-ray source is 71°. Low-resolution survey spectra were acquired between binding energies of 1-1100 eV. Higher-resolution detailed scans, with a resolution of ~ 0.8 eV, were collected on individual XPS lines of interest. The sample chamber was maintained at < 2×10^{-9} Torr. The XPS data were analyzed using the CasaXPS software.

Brunauer–Emmett–Teller (BET) was collected using a Nova 2200e surface area and pore size analyzer (Quantachrome Instruments, Inc.). Materials were degassed for 2 h at 150 °C in vacuum before measurement.

Computational Methods

All calculations were run using the *Q-CHEM* program package.[84] Geometry optimizations were run with restricted DFT calculations at the M06 level of theory with a composite basis set. The Pople 6-31G* basis set was used for H,C,N, and O atoms and the Hay–Wadt VDZ (n+1) effective core potentials and basis sets (LANL2DZ) were used for Cl and Re atoms.[85-92] All optimized geometries were verified as stable minima with frequency calculations at the same level of theory. The M06 functional was used throughout this study, as it provides reduced Hartree-Fock exchange contributions and includes empirical fitting for accuracy in organometallic systems.[93] Single point energy calculations were run with a larger 6-311G** basis for H, C, N, and O atoms and solvation was treated with COSMO (dielectric constant of 37.5 for acetonitrile).[94] Kohn-Sham orbital images are presented with isovalues of 0.05 for clarity.

Synthesis of Re(2,2'-bpy-5,5'-diamine)(CO)$_3$Cl (1)

A 100 mL oven dried 3-neck flask fitted with a reflux condenser, adaptors, and a stir bar was allowed to cool down under vacuum. The flask was then refilled with nitrogen and charged with $Re(CO)_5Cl$ (109 mg, 0.30 mmol) and toluene (45 mL). A warm (50 °C) solution of 5,5'-diamine-2,2'-bpy (55.9 mg, 0.30 mmol) in methanol (5 mL) was cannula transferred to the 3-neck flask. The reaction mixture was refluxed for 1 h. The colour of the reaction mixture changed from light to bright yellow, characteristic of the formation of the $Re(CO)_3$ species. The reaction mixture was allowed to cool to room temperature and then placed in the freezer (-29°C) overnight. A yellow precipitate formed and was collected on a glass frit, washed with 1 mL of cold methanol and dried under vacuum to afford a bright yellow solid (141 mg, yield = 95%). ^{1}H NMR (400 MHz, DMSO-d_6) δ 8.22 (d, 2H, ^4J = 2.4 Hz), 7.96 (d, 2H, ^3J = 8.8 Hz), 7.21 (dd, 2H, ^3J = 8.8 Hz, ^4J = 2.4 Hz), 6.20 (s, 4H). Anal. Calcd for $C_{13}H_{10}ClN_4O_3Re$: C, 31.74; H, 2.05, N, 11.39. Found: C, 31.94; H, 1.97; N, 11.35. X-ray quality crystals were grown by vapor diffusion of a diethyl ether/dimethylformamide mixture at room temperature over the course of 1 day.

Synthesis of Re(2,2'-bpy-5,5'-diamine)(CO)$_3$(MeCN)(OTf) (1^{OTf})

A reported procedure was followed.[74] A 3-neck flask fitted with a reflux condenser, adaptors, and a stir bar was charged with Re(2,2'-bpy-5,5'-diamine)$(CO)_3$Cl (**1**) (24.9 mg, 0.051 mmol), AgOTf (13.0 mg, 0.051 mmol), and acetonitrile (5 mL). The flask was covered with aluminium foil and the reaction mixture was allowed to stir under reflux for 24 h, during which a white precipitate formed. The supernatant was filtered, and diffusion with diethyl ether resulted in the formation of amber crystals, that were washed and dried (24.0 mg, yield = 79%). ^{1}H NMR (400 MHz, MeCN-d_3) δ 8.33 (d, 2H), 7.85 (d, 2H), 7.34 (dd, 2H), 5.05 (s, 4H), and 2.09 (s, 3H, CH_3CN). Anal. Calcd for $C_{16}H_{13}F_3N_5O_6ReS$: C, 29.72; H, 2.03; N, 10.83. Found: C, 30.12; H, 2.04; N, 10.86.

Synthesis of Zn(2,2'-bpy-5,5'-diamine)$(CH_3COO)_2 \cdot H_2O$.

A solution of 2,2'-bpy-5,5'-diamine (9.3 mg, 0.050 mmol) in 1 mL of MeOH was added to a vial with a solution of $Zn(CH_3COO)_2 \cdot 2H_2O$ (21.9 mg, 0.100 mmol) in 1 mL of water at room temperature. The reaction mixture was stirred for 1 h. Methanol was allowed to evaporate over the period of 2 days, leading to the appearance of colourless crystals, that were washed with water and dried under vacuum at 100°C (16.3 mg, 84%). ^{1}H NMR (400 MHz, DMSO-d_6) δ 8.01 (d, 2H), 7.97 (d, 2H), 7.23 (dd, 2H), 6.09 (s, 4H), and 1.79 (s, 6H, CH_3COO). Anal. Calcd for $C_{14}H_{18}N_4O_5Zn$: C, 43.37; H, 4.68; N, 14.45. Found: C, 43.30; H, 4.36; N, 14.32.

Typical synthesis of COF-2,2'-bpy-Re

Solid COF-2,2'-bpy (87.1 mg) was transferred to a 100 mL round bottom flask equipped with a magnetic stir bar and a reflux condenser. A solution of $Re(CO)_5Cl$ (108.6 mg, 1.5 equivalents) in toluene (10 mL) was added to the reaction mixture and heated at reflux temperature for 3 days. A color change was observed from red-orange to dark-red. The resulting powder was collected on a medium porosity frit and washed with acetone (3 × 10 mL), dichloromethane (3 × 10 mL), tetrahydrofurane (3 × 10 mL), and acetone (3 × 10 mL).

Additionally, the powder was washed with copious amounts of acetone to remove unreacted starting materials. The resulting powder was dried at 150°C under high vacuum for 4 h. According to ICP-OES the sample contains 29.38 mass% of Re. For other wt % Re, the synthesis was performed analogously to the original synthesis of COF-2,2'-bpy-Re (see above), with the exception that the following equivalents of the rhenium precursor were used: 0.01, 0.05, 0.15, 1.0 equivalents, or 0.7, 3.6, 10.9, and 72.4 mg, respectively. According to ICP-OES the samples contain 0.21, 0.65, 1.86, and 15.39 wt % Re, respectively.

Electrode fabrication (carbon ink method)

Glassy carbon plate electrodes (6 cm × 1 cm × 0.3 cm, Tokai Carbon Co., Ltd.) were polished with MicroPolish Powder 0.05 micron (CH Instruments, Inc.), rinsed with Millipore water and acetone, and dried. A carbon black/PVDF paste was prepared by combining 70 mg of the commercial carbon black material (Vulcan XC-72R; Fuel Cell Store), 10 mg poly(vinylidene fluoride) (Sigma-Aldrich), 20 mg COF-2,2'-bpy-Re and 4 mL of freshly distilled *N*-methyl-2-pyrrolidone (NMP). The resulting mixture was sonicated for 3 hours. Acetonitrile (10 μL) was added to the 6 cm × 1 cm electrode surface area, followed by the addition of 40 μL of the carbon black/PVDF paste per 2.5 cm^2. The electrode was allowed to dry under vacuum for 2 hours.

Electrochemical methods

Electrochemistry experiments were carried out using a Pine WaveDriver 20 Bipotentiostat. The electrochemical experiments were performed in a three-electrode configuration electrochemical cell under N_2 or CO_2 saturated atmospheres in 0.1 M tetrabutylammonium hexafluorophosphate acetonitrile solution using glassy carbon electrodes as the working electrode. Cyclic voltammetry experiments of **1** (0.5 mM) were carried out in a single compartment cell using a 3 mm glassy carbon electrode as the working electrode, platinum wire, purchased from Alfa Aesar, as the auxiliary electrode, and silver wire as the reference electrode. Controlled potential electrolysis (CPE) experiments of **1** and all electrochemical measurements for COF-2,2'-bpy and COF-2,2'-bpy-Re were conducted in a two-chambered H cell. The first chamber held the working and reference electrodes in 50 mL of 0.1 M tetrabutylammonium hexafluorophosphate in acetonitrile. The second chamber held the auxiliary electrode in 20 mL of 0.1 M tetrabutylammonium hexafluorophosphate in MeCN. The two chambers were separated by a fine porosity glass frit. The reference electrode (silver wire) was placed in a separate compartment charged with 0.1 M tetrabutylammonium hexafluorophosphate in acetonitrile, and connected by a Vycor tip. Glassy carbon plate electrodes (6 cm × 1 cm × 0.3 cm; Tokai Carbon USA) were used as the working and auxiliary electrodes. All electrochemical experiments presented here were referenced relative to ferrocene (Fc) with the $Fe^{3+/2+}$ couple at 0.0 V. Decamethylferrocene (Fc*) with the $Fe^{3+/2+}$ couple at –0.48 V was used as an internal standard.

Gas analysis for controlled potential electrolysis experiments were performed using 2 mL sample taken from the headspace of the electrochemical cell and injected into a gas chromatography instrument (Shimadzu BID-2010 plus series gas chromatograph) equipped with a BID detector and a 2 m × 1 mm Restek ShinCarbon ST Micropacked column. Faradaic efficiencies were determined by dividing the measured CO produced by the amount of CO expected based on the charge passed during the bulk electrolysis experiment. For each species the controlled-potential electrolysis measurements were performed at least twice, leading to similar behaviour. The reported Faradaic efficiencies and μmol of CO produced are average values.

Conflicts of interest

There are no conflicts to declare.

Acknowledgements

The authors are grateful to the University of Southern California (USC) and the USC Wrigley Institute for the Norma and Jerol Sonosky summer fellowship to D. A. P. The studies of the molecular complex were supported by the National Science Foundation (NSF) through the CAREER award (CHE-1555387), and the studied of the extended frameworks were supported by the Nanoporous Materials Genome Center of the U.S. Department of Energy, Office of Basic Energy Sciences, Division of Chemical Sciences, Geosciences and Biosciences under Award DE-FG02-17ER16362. The authors thank Patrick Cottingham and Andrew Clough for assistance with BET and XPS, respectively. XPS data were collected at the Center for Electron Microscopy and Microanalysis (CEMMA) at USC. This work used the Extreme Science and Engineering Discovery Environment (XSEDE), which is supported by National Science Foundation grant number ACI-1548562. All calculations were performed on the COMET cluster operated by the San Diego Supercomputer Center at UC San Diego.

References

1. T. Cook, D. Dogutan, S. Reece, Y. Surendranath, T. Teets and D. Nocera, *Chem. Rev.*, 2010, **110**, 6474.
2. E. Benson, C. Kubiak, A. Sathrum and J. Smieja, *Chem. Soc. Rev.*, 2009, **38**, 89.
3. A. Appel, J. Bercaw, A. Bocarsly, H. Dobbek, D. DuBois, M. Dupuis, J. Ferry, E. Fujita, R. Hille, P. Kenis, C. Kerfeld, R. Morris, C. Peden, A. Portis, S. Ragsdale, T. Rauchfuss, J. Reek, L. Seefeldt, R. Thauer and G. Waldrop, *Chem. Rev.*, 2013, **113**, 6621.
4. A. Morris, G. Meyer and E. Fujita, *Acc. Chem. Res.*, 2009, **42**, 1983.
5. M. Dubois and D. Dubois, *Acc. Chem. Res.*, 2009, **42**, 1974.

6. J. Concepcion, R. House, J. Papanikolas and T. Meyer, *Proc. Natl. Acad. Sci. USA*, 2012, **109**, 15560.
7. J. Collin and J. Sauvage, *Coord. Chem. Rev.*, 1989, **93**, 245.
8. C. Costentin, M. Robert and J. Saveant, *Chem. Soc. Rev.*, 2013, **42**, 2423.
9. J. Saveant, *Chem. Rev.*, 2008, **108**, 2348.
10. U. Schubert, A. Winter, G. Newkome, U. Schubert, A. Winter and G. Newkome, *Terpyridine Based Materials: For Catalytic, Optoelectronic and Life Science Applications*, 2011, 1.
11. C. Kaes, A. Katz and M. Hosseini, *Chem. Rev.*, 2000, **100**, 3553.
12. C. Scarborough, K. Lancaster, S. DeBeer, T. Weyhermueller, S. Sproules and K. Wieghardt, *Inorg. Chem.*, 2012, **51**, 3718.
13. M. Wang, J. England, T. Weyhermuller and K. Wieghardt, *Inorg. Chem.*, 2014, **53**, 2276.
14. J. Hawecker, J. Lehn and R. Ziessel, *J. Chem. Soc., Chem. Commun.*, 1984, 328.
15. T. Yoshida, T. Iida, T. Shirasagi, R. Lin and M. Kaneko, *J. Electroanal. Chem.*, 1993, **344**, 355.
16. J. Smieja and C. Kubiak, *Inorg. Chem.*, 2010, **49**, 9283.
17. S. Meshitsuka, M. Ichikawa and K. Tamaru, *J. Chem. Soc., Chem. Commun.*, 1974, 158.
18. C. Lieber and N. Lewis, *J. Am. Chem. Soc.*, 1984, **106**, 5033.
19. J. Walsh, G. Neri, C. Smith and A. Cowan, *Chem. Commun.*, 2014, **50**, 12698.
20. B. McNicholas, J. Blakemore, A. Chang, C. Bates, W. Kramer, R. Grubbs and H. Gray, *J. Am. Chem. Soc.*, 2016, **138**, 11160.
21. J. Blakemore, A. Gupta, J. Warren, B. Brunschwig and H. Gray, *J. Am. Chem. Soc.*, 2013, **135**, 18288.
22. P. Kang, S. Zhang, T. Meyer and M. Brookhart, *Angew. Chem. Int. Ed.*, 2014, **53**, 8709.
23. B. Reuillard, K. Ly, T. Rosser, M. Kuehnel, I. Zebger and E. Reisner, *J. Am. Chem. Soc.*, 2017, **139**, 14425.
24. T. Atoguchi, A. Aramata, A. Kazusaka and M. Enyo, *J. Electroanal. Chem.*, 1991, **318**, 309.
25. N. Elgrishi, S. Griveau, M. Chambers, F. Bedioui and M. Fontecave, *Chem. Commun.*, 2015, **51**, 2995.
26. S. Oh, J. Gallagher, J. Miller and Y. Surendranath, *J. Am. Chem. Soc.*, 2016, **138**, 1820.
27. T. Yoshida, K. Kamato, M. Tsukamoto, T. IIda, D. Schlettwein, D. Wohrle and M. Kaneko, *J. Electroanal. Chem.*, 1995, **385**, 209.
28. W. Kramer and C. McCrory, *Chem. Sci.*, 2016, **7**, 2506.
29. A. Guadalupe, D. Usifer, K. Potts, H. Hurrell, A. Mogstad and H. Abruna, *J. Am. Chem. Soc.*, 1988, **110**, 3462.
30. T. Otoole, L. Margerum, T. Westmoreland, W. Vining, R. Murray and T. Meyer, *J. Chem. Soc., Chem. Commun.*, 1985, 1416.
31. T. Otoole, B. Sullivan, M. Bruce, L. Margerum, R. Murray and T. Meyer, *J. Electroanal. Chem.*, 1989, **259**, 217.
32. R. Hinogami, S. Yotsuhashi, M. Deguchi, Y. Zenitani, H. Hashiba and Y. Yamada, *ECS Electrochem. Lett.*, 2012, **1**, H17.
33. I. Hod, M. Sampson, P. Deria, C. Kubiak, O. Farha and J. Hupp, *ACS Catal.*, 2015, **5**, 6302.
34. S. Lin, C. Diercks, Y. Zhang, N. Kornienko, E. Nichols, Y. Zhao, A. Paris, D. Kim, P. Yang, O. Yaghi and C. Chang, *Science*, 2015, **349**, 1208.
35. N. Kornienko, Y. Zhao, C. Kiley, C. Zhu, D. Kim, S. Lin, C. Chang, O. Yaghi and P. Yang, *J. Am. Chem. Soc.*, 2015, **137**, 14129.
36. A. Clough, J. Yoo, M. Mecklenburg and S. Marinescu, *J. Am. Chem. Soc.*, 2015, **137**, 118.
37. C. Downes and S. Marinescu, *J. Am. Chem. Soc.*, 2015, **137**, 13740.
38. R. Dong, M. Pfeffermann, H. Liang, Z. Zheng, X. Zhu, J. Zhang and X. Feng, *Angew. Chem. Int. Ed.*, 2015, **54**, 12058.
39. C. Downes and S. Marinescu, *Chemsuschem*, 2017, **10**, 4374.
40. P. Usov, S. Ahrenholtz, W. Maza, B. Stratakes, C. Epley, M. Kessinger, J. Zhu and A. Morris, *J. Mater. Chem. A*, 2016, **4**, 16818.
41. P. Usov, B. Huffman, C. Epley, M. Kessinger, J. Zhu, W. Maza and A. Morris, *ACS Appl. Mater. Interfaces*, 2017, **9**, 33539.
42. J. Zhu, W. Maza and A. Morris, *J. Photochem. Photobiol.*, 2017, **344**, 64.
43. S. Pullen, H. Fei, A. Orthaber, S. Cohen and S. Ott, *J. Am. Chem. Soc.*, 2013, **135**, 16997.
44. S. Pullen and S. Ott, *Top. Catal.*, 2016, **59**, 1712.
45. E. Mijangos, S. Roy, S. Pullen, R. Lomoth and S. Ott, *Dalton Trans.*, 2017, **46**, 4907.
46. B. Johnson, A. Bhunia and S. Ott, *Dalton Trans.*, 2017, **46**, 1382.
47. L. Ye, J. Liu, Y. Gao, C. Gong, M. Addicoat, T. Heine, C. Woll and L. Sun, *J. Mater. Chem. A*, 2016, **4**, 15320.
48. C. Wang, Z. Xie, K. deKrafft and W. Lin, *J. Am. Chem. Soc.*, 2011, **133**, 13445.
49. A. Blake, N. Champness, T. Easun, D. Allan, H. Nowell, M. George, J. Jia and X. Sun, *Nat. Chem.*, 2010, **2**, 688.
50. H. Fei, M. Sampson, Y. Lee, C. Kubiak and S. Cohen, *Inorg. Chem.*, 2015, **54**, 6821.
51. C. Hendon, J. Bonnefoy, E. Quadrelli, J. Canivet, M. Chambers, G. Rousse, A. Walsh, M. Fontecave and C. Mellot-Draznieks, *Chem. Eur. J.*, 2016, **22**, 3713.
52. S. Lin, Y. Pineda-Galvan, W. A. Maza, C. C. Epley, J. Zhu, M. C. Kessinger, Y. Pushkar and A. J. Morris, 2017, **- 10**.
53. S. Lin, A. K. Ravari, J. Zhu, P. Usov, M. Cai, S. R. Ahrenholtz, Y. Pushkar and A. Morris, *ChemSusChem*, n/a.
54. C. DeBlase, K. Silberstein, T. Truong, H. Abruna and W. Dichtel, *J. Am. Chem. Soc.*, 2013, **135**, 16821.
55. S. Chandra, S. Kandambeth, B. Biswal, B. Lukose, S. Kunjir, M. Chaudhary, R. Babarao, T. Heine and R. Banerjee, *J. Am. Chem. Soc.*, 2013, **135**, 17853.
56. H. Aiyappa, J. Thote, D. Shinde, R. Banerjee and S. Kurungot, *Chem. Mater.*, 2016, **28**, 4375.
57. C. N. R. Rao and R. Venkataraghavan, *Spectrochim. Acta*, 1962, **18**, 273.
58. B. Sullivan, C. Bolinger, D. Conrad, W. Vining and T. Meyer, *J. Chem. Soc., Chem. Commun.*, 1985, 1414.
59. S. Slater and J. Wagenknecht, *J. Am. Chem. Soc.*, 1984, **106**, 5367.
60. C. Bolinger, B. Sullivan, D. Conrad, J. Gilbert, N. Story and T. Meyer, *J. Chem. Soc., Chem. Commun.*, 1985, 796.
61. C. Costentin, S. Drouet, M. Robert and J. Saveant, *J. Am. Chem. Soc.*, 2012, **134**, 19949.

62. A. Chapovetsky, T. Do, R. Haiges, M. Takase and S. Marinescu, *J. Am. Chem. Soc.*, 2016, **138**, 5765.
63. A. Chapovetsky, M. Welborn, J. Luna, R. Haiges, T. Miller and S. Marinescu, *ACS Cent. Sci.*, 2018, **4**, 397.
64. M. Clark, P. Cheung, M. Lessio, E. Carter and C. Kubiak, *ACS Catal.*, 2018, **8**, 2021.
65. E. Benson, K. Grice, J. Smieja and C. Kubiak, *Polyhedron*, 2013, **58**, 229.
66. E. Benson and C. Kubiak, *Chem. Commun.*, 2012, **48**, 7374.
67. K. Grice, N. Gu, M. Sampson and C. Kubiak, *Dalton Trans.*, 2013, **42**, 8498.
68. J. Keith, K. Grice, C. Kubiak and E. Carter, *J. Am. Chem. Soc.*, 2013, **135**, 15823.
69. C. Machan, M. Sampson, S. Chabolla, T. Dang and C. Kubiak, *Organometallics*, 2014, **33**, 4550.
70. Y. Hayashi, S. Kita, B. Brunschwig and E. Fujita, *J. Am. Chem. Soc.*, 2003, **125**, 11976.
71. J. Agarwal, E. Fujita, H. Schaefer and J. Muckerman, *J. Am. Chem. Soc.*, 2012, **134**, 5180.
72. P. Christensen, A. Hamnett, A. Muir and J. Timney, *J. Chem. Soc., Dalton Trans.*, 1992, 1455.
73. E. E. Benson, M. D. Sampson, K. A. Grice, J. M. Smieja, J. D. Froehlich, D. Friebel, J. A. Keith, E. A. Carter, A. Nilsson and C. P. Kubiak, *Angew. Chem. Int. Ed.*, 2013, **52**, 4841.
74. J. Smieja, E. Benson, B. Kumar, K. Grice, C. Seu, A. Miller, J. Mayer and C. Kubiak, *Proc. Natl. Acad. Sci. USA*, 2012, **109**, 15646.
75. D. Shinde, H. Aiyappa, M. Bhadra, B. Biswal, P. Wadge, S. Kandambeth, B. Garai, T. Kundu, S. Kurungot and R. Banerjee, *J. Mater. Chem. A*, 2016, **4**, 2682.
76. Z. Wang and S. Cohen, *Chem. Soc. Rev.*, 2009, **38**, 1315.
77. S. Cohen, *Chem. Rev.*, 2012, **112**, 970.
78. S. Cohen, *J. Am. Chem. Soc.*, 2017, **139**, 2855.
79. I. Stassen, N. Burtch, A. Talin, P. Falcaro, M. Allendorf and R. Ameloot, *Chem. Soc. Rev.*, 2017, **46**, 3853.
80. L. Sun, M. Campbell and M. Dinca, *Angew. Chem. Int. Ed.*, 2016, **55**, 3566.
81. M. Albrecht, I. Janser, A. Lutzen, M. Hapke, R. Frohlich and P. Weis, *Chem. Eur. J.*, 2005, **11**, 5742.
82. Q. Sun, B. Aguila, J. Perman, N. Nguyen and S. Ma, *J. Am. Chem. Soc.*, 2016, **138**, 15790.
83. J. Chong, M. Sauer, B. Patrick and M. MacLachlan, *Org. Lett.*, 2003, **5**, 3823.
84. Y. Shao, L. Molnar, Y. Jung, J. Kussmann, C. Ochsenfeld, S. Brown, A. Gilbert, L. Slipchenko, S. Levchenko, D. O'Neill, R. DiStasio, R. Lochan, T. Wang, G. Beran, N. Besley, J. Herbert, C. Lin, T. Van Voorhis, S. Chien, A. Sodt, R. Steele, V. Rassolov, P. Maslen, P. Korambath, R. Adamson, B. Austin, J. Baker, E. Byrd, H. Dachsel, R. Doerksen, A. Dreuw, B. Dunietz, A. Dutoi, T. Furlani, S. Gwaltney, A. Heyden, S. Hirata, C. Hsu, G. Kedziora, R. Khalliulin, P. Klunzinger, A. Lee, M. Lee, W. Liang, I. Lotan, N. Nair, B. Peters, E. Proynov, P. Pieniazek, Y. Rhee, J. Ritchie, E. Rosta, C. Sherrill, A. Simmonett, J. Subotnik, H. Woodcock, W. Zhang, A. Bell, A. Chakraborty, D. Chipman, F. Keil, A. Warshel, W. Hehre, H. Schaefer, J. Kong, A. Krylov, P. Gill and M. Head-Gordon, *Phys. Chem. Chem. Phys.*, 2006, **8**, 3172.
85. R. Ditchfield, W. Hehre and J. Pople, *J. Chem. Phys.*, 1971, **54**, 724.
86. P. Harihara and J. Pople, *Theor. Chim. Acta*, 1973, **28**, 213.
87. W. Hehre, R. Ditchfield and J. Pople, *J. Chem. Phys.*, 1972, **56**, 2257.
88. D. Feller, *J. Comput. Chem.*, 1996, **17**, 1571.
89. K. Schuchardt, B. Didier, T. Elsethagen, L. Sun, V. Gurumoorthi, J. Chase, J. Li and T. Windus, *J. Chem. Inf. Model*, 2007, **47**, 1045.
90. J. Towns, T. Cockerill, M. Dahan, I. Foster, K. Gaither, A. Grimshaw, V. Hazlewood, S. Lathrop, D. Lifka, G. Peterson, R. Roskies, J. Scott and N. Wilkins-Diehr, *Comut. Sci. Eng.*, 2014, **16**, 62.
91. P. Hay and W. Wadt, *J. Chem. Phys.*, 1985, **82**, 270.
92. W. Wadt and P. Hay, *J. Chem. Phys.*, 1985, **82**, 284.
93. Y. Zhao and D. Truhlar, *Theor. Chem. Acc.*, 2008, **120**, 215.
94. A. Klamt and G. Schuurmann, *J. Chem. Soc., Perkin Trans. 1*, 1993, 799.

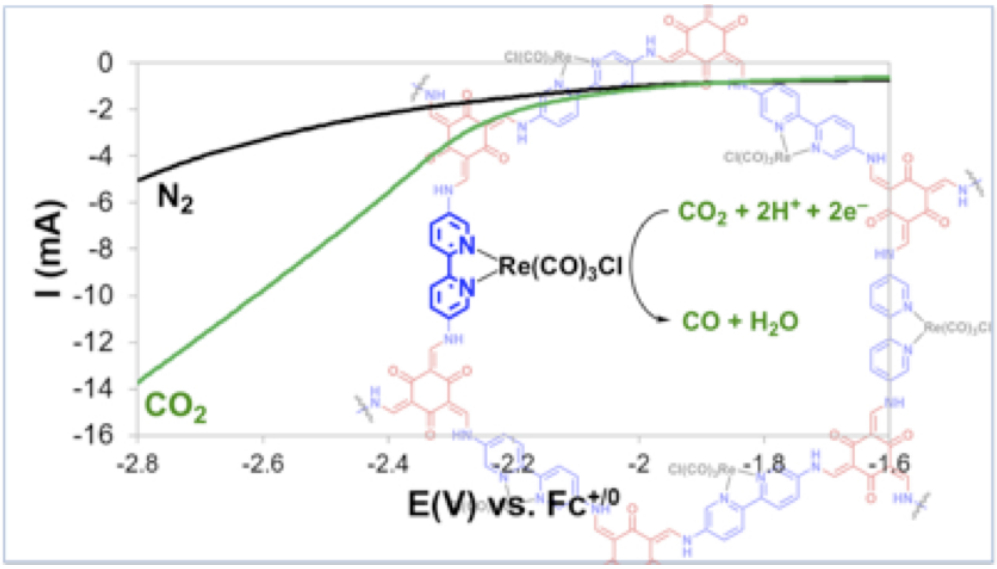
0
-2
-4
-6
-8
-10
-12
-14
-16
I (mA)
N2
CO2
-2.8
-2.6
-2.4
-2.2
-2
-1.8
-1.6
E(V) vs. Fc+/0
Re(CO)3Cl
CO2 + 2H+ + 2e−
CO + H2O